Title:

High-throughput cellular heterogeneity analysis in cell migration at the single-cell level.

Authors:

Mengli Zhou[a,b,c], Yushu Ma[a,b], Chun-Cheng Chiang[a,b], Edwin C. Rock[d], Kathryn E. Luker[e], Gary D. Luker[e,f,g], Yu-Chih Chen[a,b,d,h*]

a UPMC Hillman Cancer Center, University of Pittsburgh, 5115 Centre Ave, Pittsburgh, PA 15232, USA;

b Department of Computational and Systems Biology, University of Pittsburgh, 3420 Forbes Avenue, Pittsburgh, PA 15260, USA;

c Xiangya Hospital, Central South University, Changsha, Hunan, 410008, China;

d Department of Bioengineering, Swanson School of Engineering, University of Pittsburgh, 3700 O'Hara Street, Pittsburgh, PA 15260, USA;

e Center for Molecular Imaging, Department of Radiology, University of Michigan, 109 Zina Pitcher Place, Ann Arbor, MI 48109-2200, USA;

f Department of Microbiology and Immunology, University of Michigan, 109 Zina Pitcher Place, Ann Arbor, MI 48109-2200, USA;

g Department of Biomedical Engineering, University of Michigan, 2200 Bonisteel, Blvd. Ann Arbor, MI 48109-2099, USA

h CMU-Pitt Ph.D. Program in Computational Biology, University of Pittsburgh, 3420 Forbes Avenue, Pittsburgh, PA 15260, USA

*Corresponding authors

Yu-Chih Chen

5115 Centre Ave, Pittsburgh, PA 15232, USA

Tel: 412-623-7701; E-mail: cheny25@upmc.edu.

Abstract

Cancer cell migration represents an essential step toward metastasis and cancer deaths. However, conventional drug discovery focuses on cytotoxic and growth-inhibiting compounds rather than inhibitors of migration. Drug screening assays generally measure the average response of many cells, masking distinct cell populations that drive metastasis and resist treatments. Here, we developed a high-throughput microfluidic migration platform that coordinates robotic liquid handling and computer vision for rapidly quantifying individual cellular motility. Using this innovative technology, we tested 172 compounds and found a surprisingly low correlation between migration and growth inhibition. Notably, we discovered that many compounds inhibited migration of most cells while leaving fast-moving subpopulations. We further pinpointed synergistic drug combinations, including Bortezomib and Danirixin, to stop fast-moving cells. To explain the observed cell behaviors, we performed single-cell morphological and molecular analysis. These studies establish a novel technology to identify promising migration inhibitors for cancer treatment and relevant applications.

Keywords: Cell migration, Single-cell analysis, Microfluidics, Breast cancer, Metastasis, Image processing

Introduction

Metastasis is the major cause of breast cancer deaths, accounting for over 40,000 deaths per year in the US. Despite advances in early detection and treatment, once metastases develop, breast cancer remains incurable.[1,2] While cancer metastasis is a complicated multi-step process, migration and intravasation of tumor cells from the tumor stroma to a capillary bed or lymphatic vessel represent critical early steps.[3] In addition, considerable evidence suggests that cancer metastasis can be driven by epithelial-to-mesenchymal transition (EMT),[4-6] a developmental program in which epithelial cells acquire migratory and invasive phenotypes.[7-10] Inhibition or activation of EMT significantly limits or increases metastasis, respectively.[11-13] To elucidate the correlation between cancer migration and metastasis, we previously developed a high-throughput microfluidic platform that can measure the individual migratory capability of thousands of cancer cells and selectively isolate fast-moving subpopulations.[14,15] As expected, we found that highly migratory breast cancer cells metastasized more than non-migratory cells.[15] Furthermore, through whole transcriptome sequencing of migratory and control cancer cells, differentially expressed genes that correlate with clinical outcomes in breast cancer were identified.[16] The distinct gene expression profile of migratory cancer cells highlights the possibility to selectively inhibit this metastatic sub-population. As migratory breast cancer cells are key contributors to metastatic dissemination, we expect that inhibition of cell migration can reduce the metastatic burden of breast cancer.[15,17,18]

Despite the importance of cancer cell migration in metastasis, it has been neglected in conventional drug discovery. Conventional drug screening focuses mainly on compounds that significantly inhibit cell viability and/or growth.[19] For instance, NCI-60 Human Tumor Cell Lines Screen first performed a one-dose assay to quantify growth inhibition and lethality of compounds. The compounds that do not exhibit significant growth inhibition were not considered further. However, compounds that inhibit cell migration might have potent clinical value for metastatic disease. While there are some previous trials targeting cell functions relevant to migration, including protease, integrin, and extracellular matrix (ECM), there is no systematic screening for cell migration inhibitors.[20-25] More importantly, the screening experiments generally measure the responses of many cells in bulk, masking a small number of distinct cells that may drive metastasis.[11-13]

Cellular heterogeneity is a hallmark of multicellular life which presents various forms and functions in organisms by facilitating specialization. This heterogeneity controls physiological processes of normal cells as well as pathological conditions of many diseases.[26,27] However, most of our current biological knowledge is based on population-averaged measurements.

While bulk analysis of many cells altogether measures the overall cellular responses, regulations and mechanisms, the baseline assumption that all cells are identical can lead to imprecise and often incorrect assessments.[28] With new engineering tools having single-cell resolution, it has become clear that cell-to-cell variability is pervasive and critical.[29] Cancer as a genetic disease has an abnormal and unstable genome and epigenome.[30] The instability can be caused by erroneous DNA repair mechanisms and an abnormal tumor micro-environment, which is hypoxic, acidic, and lacks nutrition.[31,32] This molecular-level instability leads to inter-patient and intra-patient tumor heterogeneity and generates formidable challenges in identifying optimal treatments.[28,33,34]

Popular established cell migration assays, such as wound healing and transwells, have limited utility for detecting single-cell heterogeneity.[35,36] Wound healing assays present challenges both in the reproducibility of the scratch and the difficulty tracking individual cells.[37] Transwell assays provide a binary migration measurement of cells, but tracking the actual cell movement process is not possible. These fundamental limitations hinder the study of cellular heterogeneity and dynamics of cell migration. Due to the features of small reagent volumes, precise fluid control, and small device footprint, microfluidics has emerged as a cutting-edge technology to monitor the movement of individual cells.[14-18,38-45] Despite significantly better single-cell tracking capability of microfluidic platforms, most existing devices are not readily compatible and coordinated with robotic liquid handling and image processing for high-throughput screening. To identify potent cell migration inhibitors and consider cellular heterogeneity, there is an unmet need to measure single-cell motility in high throughput and at low cost. To address the limitations of existing platforms, we developed a high-throughput microfluidic migration platform for tracking the movement of thousands of cells. We focused on triple-negative breast cancer (TNBC), which is more aggressive and has few targeted therapies.[46,47] Utilizing the cutting-edge screening capability of our system, we screened a custom library of 172 compounds to identify compounds that specifically inhibited cell migration, cell proliferation, or both. The experiments suggest that inhibition of cell migration and proliferation are not highly correlated, so conventional drug screening experiments might overlook promising migration inhibitors. In addition to the mean cell migration capacity, we characterized the movement of top-ranked fast-moving cells. Interestingly, we found many compounds that inhibited the migration of most cells but not fast-moving ones. The cellular heterogeneity would not be revealed without individual cell tracking. Based on the throughput of the presented method, we tested drug combinations to stop the movement of fast-moving cells. We also performed single-cell morphological and molecular characterization to explain the observed cell migration phenotype.

Results

High-throughput microfluidic migration assay with autonomous image processing

We developed a high-throughput microfluidic migration platform that can quantify the migration distance of 100 individual cells per condition and test 32 treatment conditions on a single device (**Fig. 1A**). After the migration assay of 24 hours, images were collected by a motorized Nikon Ti2-E fluorescence microscope. Based on our previously developed MATLAB program for quantifying cell migration, we further established an autonomous image processing toolkit with fully automatic image registration and quality control functions.[15] The image registration was performed using two features on the images. (1) The blue auto-fluorescence of Silicone on the ProPlate® 64-Well device was used to crop the region of cell migration channels. (2) The brightfield image of migration channels was used to calculate the rotation angles of images and separate individual channels (**Fig. 1B**). Based on the two features, the images can be automatically rotated and cropped for analysis. In addition, we implemented quality control functions to exclude images from defective microfluidic devices and/or poor imaging conditions. The migration devices with leakage, trapped bubbles were excluded. The over-exposed and out-of-focus images were also eliminated automatically. After quality control and image processing, the locations of cells were calculated based on cellular fluorescence. Point noise, debris, and dead cells were excluded by their small area and/or dim fluorescence. It takes around 2 seconds to process an image. The enlarged images tracking the movement of individual cells are shown in **Fig. S1**. As a proof of the concept, we compared the presented microfluidics with conventional transwell assays using the same chemoattractant of serum. The side-by-side comparison highlights the advantages of the presented method. (1) The conventional transwell assay cannot clearly distinguish the effects of cell killing and migration inhibition. As a demonstration, we treated cells with a CD4/6 inhibitor (Abemaciclib) which inhibited cancer cell growth but did not stop cell migration and an IL8 inhibitor (Danirixin) which inhibited cell migration but not growth. Transwell assays showed negative for both treatments, yet the presented microfluidic migration assay detected the differences (**Fig. 1(C-E), Table S1,S2**). (2) The microfluidic approach tracked the actual moving process of individual cells, so not only the mean cellular migration distance but also the migration distance of the top-ranked (*e.g.,* 95th percentile) fast-moving cells could be measured. (3) The transwell inserts could only test 24 conditions in the area of a well-plate (455 mm^2 per condition), while the microfluidic assay tested 32 conditions in the area of a glass slide (59 mm^2 per condition). The presented system has significantly higher throughput and saves reagents. In addition, the device matches the pitch of 384-well plate, so it is fully compatible with robotic liquid

handling. Using an Opentrons OT-2 pipetting robot, it takes 1 minute to load cells onto a device and 3 minutes to add drugs for testing 32 conditions (**Video S1**). The manual and robotic operations achieved similar experimental results (**Fig. S2**).

Correlation between growth and migration inhibition

Using the new high-throughput migration platform, we characterized the changes in cell chemotaxis toward serum when treated with a custom library of 172 compounds, including conventional chemotherapeutics, ferroptosis inducers, and inhibitors of Mitogen-activated protein kinase (MAPK), Bromodomain and extra-terminal motif (BET), Histone deacetylase (HDAC), Poly (ADP-ribose) polymerase (PARP), Human epidermal growth factor receptor 2 (HER2), Proteasome, Hypoxia-inducible factor (HIF), Aldehyde dehydrogenase (ALDH), Autophagy, Transforming growth factor-beta (TGF-β), CDK4/6, Epidermal growth factor receptor (EGFR), Nuclear factor-kappa B (NF-κB), CXCR1, CXCR4, IL8, Rho-associated protein kinase (ROCK), Colony-stimulating factor 1 receptor (CSF1R), Proto-oncogene tyrosine-protein kinase Src, p21-activated kinase (PAK), Rac, Rho, CDC42, Focal Adhesion Kinase (FAK), Wnt, Aurora, and regulators of key cellular components, including mitochondria, microtubule, integrin, kinesin, and myosin with multiple breast cancer cell lines (**Table S3,S4**). A compound concentration of 10 μM was used in the screening experiments following the NCI-60 Human Tumor Cell Lines Screen project. In addition to cell migration assays, conventional growth inhibition experiments were performed to quantify the growth inhibition and/or cytotoxicity effects of compounds for three TNBC cell lines (**Fig. 2 (A-D), Table S5**). Interestingly, we found a weak correlation between migration and growth inhibition (correlation coefficients of MDA-MB-231: 0.17, SUM149: 0.34, SUM159: 0.34). The growth inhibitors are not necessarily strong inhibitors of cell migration, and migration inhibitors might not stop cell growth. In addition to single-dose treatments, we further tested 5 concentrations of selected compounds to validate the screening experiment (**Fig. 2E, F**). We found interesting compounds, including Danirixin (GSK1325756), an IL8 inhibitor, which inhibited cell migration significantly but not cell growth, and Abemaciclib, a CDK4/6 inhibitor, which stopped cell growth but not cell migration (**Fig. 2G, H**). IL8 inhibitor (Aprepitant) and CDK4/6 inhibitors (Palbociclib HCl and Ribociclib) have consistent effects as Danirixin and Abemaciclib, respectively. Among the 172 tested compounds, 84 compounds significantly inhibited cell migration but not growth, 18 compounds significantly inhibited growth but not migration, and 56 compounds inhibited both growth and migration (**Table S6**). There are also compounds that can inhibit both cell growth and migration, including all 5 proteasome inhibitors (Bortezomib, MG-132, Carfilzomib, Ixazomib, and Ixazomib Citrate), three Src inhibitors (Saracatinib, Tirbanibulin, and Dasatinib), and 5 ferroptosis inducers (Imidazole

ketone erastin (IKE), RSL3, FINO2, ML162, and ML210) (**Fig. 2I**). The difference in cell growth and migration inhibition highlights the possibility that screening of cell migration inhibition can provide a unique list of promising compounds in cancer treatment.

Pinpointing the motility of fast-moving cells

We further investigated the movement of highly migratory cells in addition to the mean cell motility. Overall, the mean cell migration distance was correlated with that of the top 5% fast-moving cells (correlation coefficients of MDA-MB-231: 0.57, SUM149: 0.85, SUM159: 0.85) (**Fig. 3A-D**). When treating 3 TNBC cell lines with the 172 compounds, 62 compounds significantly inhibited mean cell migration but not fast-moving cells, 1 compound significantly inhibited the movement of fast-moving cells but not mean cell migration, and 78 compounds inhibited both (**Table S7, S8**). For example, Ispinesib, a potent and specific inhibitor of kinesin spindle protein (KSP), significantly slowed the movement of most cells, yet a small number of cells remained migratory (**Fig. 3E**).[48] The same situation was observed in other compounds, including Daidzin, which is a natural organic compound from soybean leaves and known to reduce ovarian and breast cancer cell migration, and SBI-0206965, an autophagy inhibitor. [49-51] In comparison, IL8 inhibitors, Danirixin and Aprepitant, and proteasome inhibitors, Carfilzomib and Bortezomib, inhibited the movement of all cells (**Fig. 3E**). [52-54] Measuring the average cell migration capacity using conventional bulk assays will not reveal these differences. In addition to single-dose treatment, we further tested 5 concentrations of selected compounds to validate the screening results. Abemaciclib neither inhibited the migration of mean nor fast-moving cells (**Fig. 3F**), and Danirixin inhibited the migration of both mean and fast-moving cells (**Fig. 3G**). More interestingly, CUDC-101, a potent multi-targeted inhibitor against HDAC, EGFR, and HER2, inhibited the migration of mean, but not fast-moving cells (**Fig. 3H**).[55] The in-depth comparison of the bulk cells versus top-ranked fast-moving ones highlights the issue of cellular heterogeneity, which has been largely overlooked in many conventional assays.

Dynamics of cell movement and the treatment combinations

In addition to a snapshot observation, the migration platform allows tracking of individual cells (**Fig. 4A**). When watching the dynamics of movement, we found a small number of fast-moving cells significantly outperformed most slow-moving cells. In literature, those fast-moving cells are reported to be the key drivers of tumor initiation and metastasis. [15,17,18] While Danirixin and Bortezomib significantly inhibited the mean cell migration distance, a small number of fasting-moving cells continued moving forward (**Fig. 4A**). The inability to stop those fast-moving cells could be explained by cancer cellular heterogeneity and the

existence of redundant pathways to circumvent the drug targets.[56] Given the limitation of mono-drug treatments, we explored the combination of drugs to completely stop highly migratory cells. We first tested the combination of the migration inhibitor of Danirixin and the growth inhibitor of Abemaciclib (**Fig. 4B**). Overall, the effects were orthogonal: the cell motility largely depended on the concentration of Danirixin, and the cell viability mostly depended on the concentration of Abemaciclib. However, we observed a strong synergistic effect on inhibiting cell migration when combining 1 μM of Danirixin and 10 μM of Abemaciclib. We also tested the combination of two cell migration inhibitors, Danirixin and Bortezomib. We found synergistic effects when combining 1-10 μM of Danirixin and 1-10 μM of Bortezomib (**Fig. 4C**). The synergistic effects also exist for inhibiting fast-moving cells (**Fig. S3**). When monitoring the cell movement over time (**Fig. 4A**), we found that cell movement was completely stopped after 6 hours by the combination of Danirixin and Bortezomib. The preliminary tests of drug combinations highlight the potential of the high-throughput platform to effectively examine combinations of compounds.

Cellular Filopodia and Actin morphology correlate with cell motility

To better understand how cell migration was inhibited, we also examined the morphology of cellular actin and filopodia. Filopodia are composed of cross-linked actin microfilament bundles and pioneer at the leading edge of migrating cells. [57,58] Therefore, increased filopodia formation has been shown to promote migration.[59] In our experiment, MDA-MB-231 cells were transfected with LifeAct-GFP for visualizing actin in filopodia. As shown in **Fig. 5 and Table S9**, the number of filopodia significantly decreased with the treatment of Danirixin or Bortezomib. At the same time, Abemaciclib treatment does not alter the number of filopodia as compared to the control. The observation of cell morphology matches well with our prior data suggesting that Danirixin and Bortezomib inhibited cell migration, while Abemaciclib did not alter cell migratory behaviors although with high cytotoxicity.

Transcriptomic effects of Abemaciclib

To better understand the unexpected effects of Abemaciclib, which inhibited cell growth but not migration, we performed scRNA-Seq to profile molecular alterations by Abemaciclib. The control and treated MDA-MB-231 cells segregated well in the UMAP plot and by altered marker genes (**Fig. 6A, B**). We identified the marker genes of Abemaciclib treatment and performed pathway analysis (**Fig. 6C, D**). Using the NCI-Nature pathway database, two groups of pathways are highlighted: (1) cell cycle signaling, including “Aurora B,” “Hepatocyte Growth Factor Receptor,” and “C-MYC transcriptional activation” and (2) cell migration regulation, including “Posttranslational regulation of adherens junction,” “N-

cadherin signaling," "E-cadherin signaling," "Nectin adhesion," and "Integrin-linked kinase signaling." Using the GO Cellular Component pathway database, we also observed the activation of cell cycle related pathways of "nucleus" and "chromosome" and cell migration related pathways of "focal adhesion" and "cell-substrate junction." The pathway analyses suggest that both cell cycle and migration are central to the difference between control and Abemaciclib treated cells. Specifically, Abemaciclib treatment significantly reduced the expression of key genes related to proliferation and cell cycle, including Marker of proliferation Ki-67 (MKI67), DNA topoisomerase II alpha (TOP2A), Centromere protein F (CENPF), Aurora Kinase A (AURKA), Cyclin B1 (CCNB1), Cyclin Dependent Kinase Inhibitor 3 (CDKN3), Pituitary tumor transforming gene 1 (PTTG1), Protein disulfide-isomerase A3 (PDIA3), Chromobox 3 (CBX3) (**Fig. 6E**).[60-65] As such, the molecular changes match well with the observed cell growth inhibition by Abemaciclib and known effects of inhibiting CDK4/6. At the same time, treatment boosted the expression of migration related genes of Vimentin (VIM), Cell division cycle protein 42 (CDC42), Actin Related Protein 2/3 Complex Subunit 4 (ARPC4).[66-69] More interestingly, the expression levels of key proteins in filopodia, including Ras Homolog Family Member A (RHOA), Ras Homolog Family Member C (RHOC), Actin Beta (ACTB), Rac Family Small GTPase 1 (RAC1), Myosins (percent.myo), Serpin Family E Member 1 (SERPINE1) remained comparable after treatment.[70-75] The elevated and unchanged expression levels in key cell migration regulators match the observation that Abemaciclib treatment did not suppress cell migration. The preliminary investigation by scRNA-Seq explains the distinct effects of Abemaciclib on cell growth and migration.

Discussion

While the importance of cancer cell migration and heterogeneity has been widely acknowledged, there is no effective way to screen cell migration with single-cell resolution in high throughput. Although conventional migration assays (*e.g.,* wound healing and transwell) are standardized for robotic operation, the assays are unable to track the movement of individual cells to study cellular heterogeneity. Microfluidic technology provides significantly better single-cell tracking capability, but most existing platforms are not readily compatible and coordinated with robotic liquid handling and image processing. In this work, we integrated user-friendly microfluidics, robotic liquid handling, and computer vision for a high-throughput migration assay at the single cell level. The platform is fully compatible with liquid handling systems. The robotic liquid handling can not only save time for researchers but also enhance the throughput and reproducibility of experiments. In addition to experiments, we establish an autonomous image processing toolkit with fully automatic image registration,

quality control, and characterization of cell migratory behaviors. With the capability, we successfully analyzed thousands of images and tracked the movement of hundreds of thousands of individual cells. While we focus on breast cancer in this study, the established technology can be widely applied to other malignancies and applications related to cell migration.

In the comparison between inhibition of cell growth and migration, we found a strikingly weak correlation. The difference can be caused by technical reasons. For example, cell migration is a 1-day experiment, while cell growth experiments last 2 days. The differences in protocol naturally introduce inconsistency. At the same time, the scRNA-Seq experiment clearly supports the distinct molecular alteration of cell growth and migration by Abemaciclib. Within 1 day of treatment, Abemaciclib successfully suppressed the cell proliferation markers of MKI67 and TOP2A.[61] The molecular changes match well with the observed growth inhibition. At the same time, the treatment enhanced the expression of VIM, CDC42, and ARPC4.[66-69] Furthermore, the expression levels of many critical genes (e.g., RHOA, RHOC, and RAC1) in cell migration filopodia were not changed, which strongly support the unchanged cell migration capacity and filopodia morphology.[70-74] The preliminary molecular investigation clearly supports that a compound can be a potent growth inhibitor but not a migration inhibitor. Given the importance of cell migration in the dissemination of cancer, the screening for cell migration inhibitors will provide an independent new list of promising compounds.

In addition to the average cell migration capacity, the platform also allows for the investigation of a small number of fast-moving cells. It was reported tens of tumor-initiating cells (TICs) are sufficient to generate a tumor in animal models.[76-79] As such, reducing the migration capacity of most cells might not be sufficient to stop cancer metastasis. In our experiments, we found that many compounds significantly inhibited the average cell motility but not the fast-moving cells, especially for the MDA-MB-231 cell line, which is known to be highly aggressive and heterogeneous.[80-82] The inability to stop those fast-moving cells might be explained by cancer cellular heterogeneity and the existence of redundant pathways. In our prior work, we have performed scRNA-Seq for highly migratory breast cancer cells.[16] While migratory cells overall demonstrate an EMT-like gene expression profile, further interrogation of migratory cells reveals discrete sub-populations expressing epithelial (CDH1, EpCAM, and cytokeratins) or mesenchymal (CDH2, VIM, SNAI2, and ZEB1) markers. Co-existence of multiple cell states within the migratory population highlights the existence of multiple layers of cellular heterogeneity. In addition to the cellular heterogeneity in motility, migratory cells can become migratory based on different molecular mechanisms. Thus, it is essential to consider the combination of multiple inhibitors to stop distinct sub-populations of

migratory cells. In this study, we performed preliminary tests to identify the synergistic combination of Danirixin and Bortezomib, which could stop the movement of all cells. The combination suppressed the potential alternative and/or redundant pathways to activate cell migration and inhibits all migratory sub-populations. To identify appropriate drug combinations in the future, it is necessary to include more candidates. The high throughput of the presented method would be the key to overcoming the experimental complexity and cost which increase exponentially.[83-86]

Figures

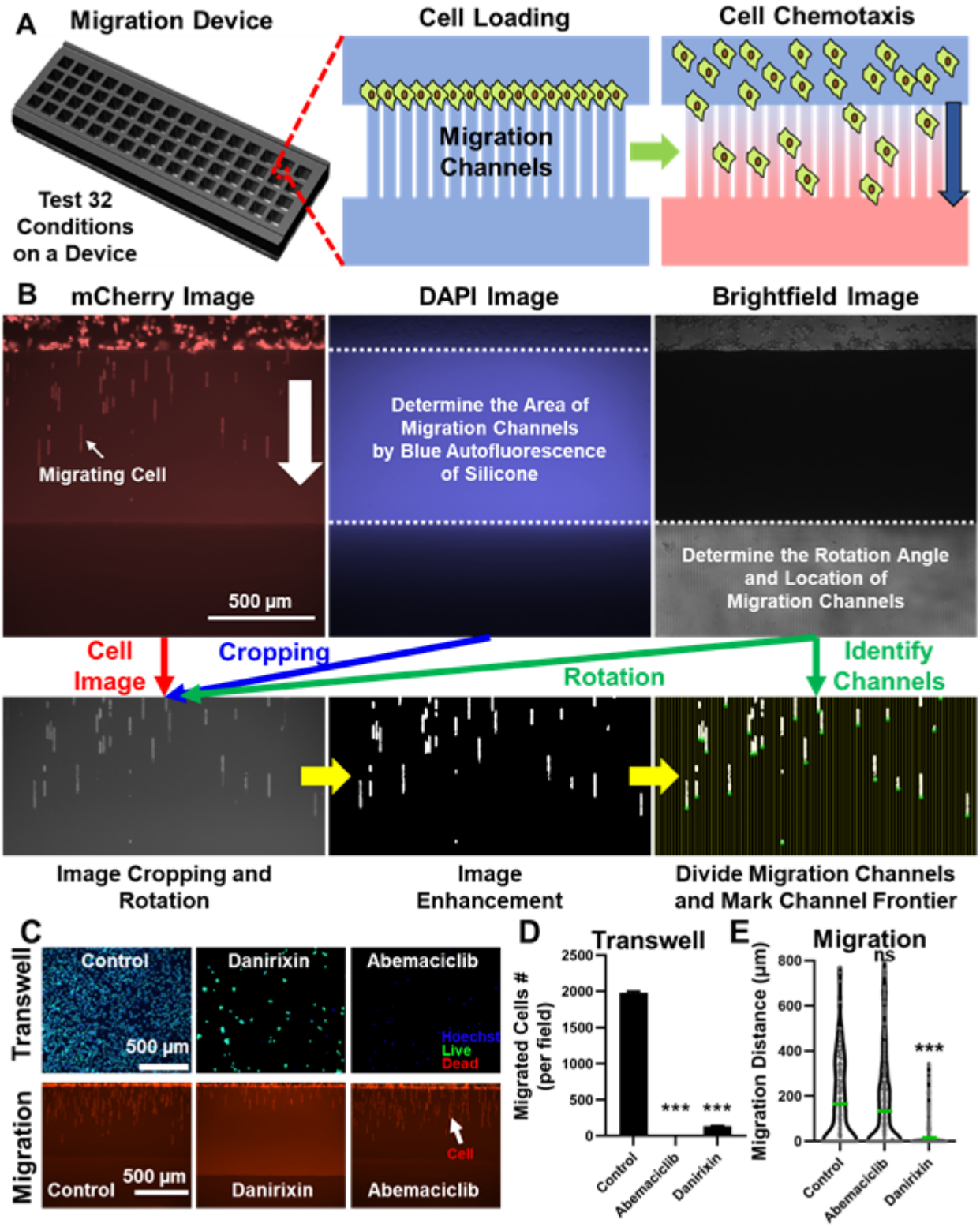

Figure 1. High-throughput microfluidic migration platform with single-cell resolution. (A) A migration device that can test 32 conditions with 100 cells per condition. Two wells are used as a pair for cell migration analysis, and the cell migration channels are between two wells. Initially, cells are loaded into the upper wells. After cell adhesion, chemoattractant is

loaded in the lower wells to induce cell migration into channels. (B) The representative images of migrating cells, Silicone outline, and migration channels for image processing. Scale bar: 500 μm. (C) The transwell and migration assays of MDA-MB-231 cells treated with DMSO control, Danirixin and Abemaciclib (10 μM for all compounds). Cells were stained with Live (green), Dead (red) and Hoechst (blue) staining reagents in the transwell experiments. Scale bar: 500 μm. (D) The transwell assay of MDA-MB-231 treated with DMSO control, Danirixin and Abemaciclib. (N = 3) (E) The microfluidic migration assay of MDA-MB-231 treated with DMSO control, Danirixin and Abemaciclib. N = 300 channels. Statistical analysis is provided in Table S1, S2.

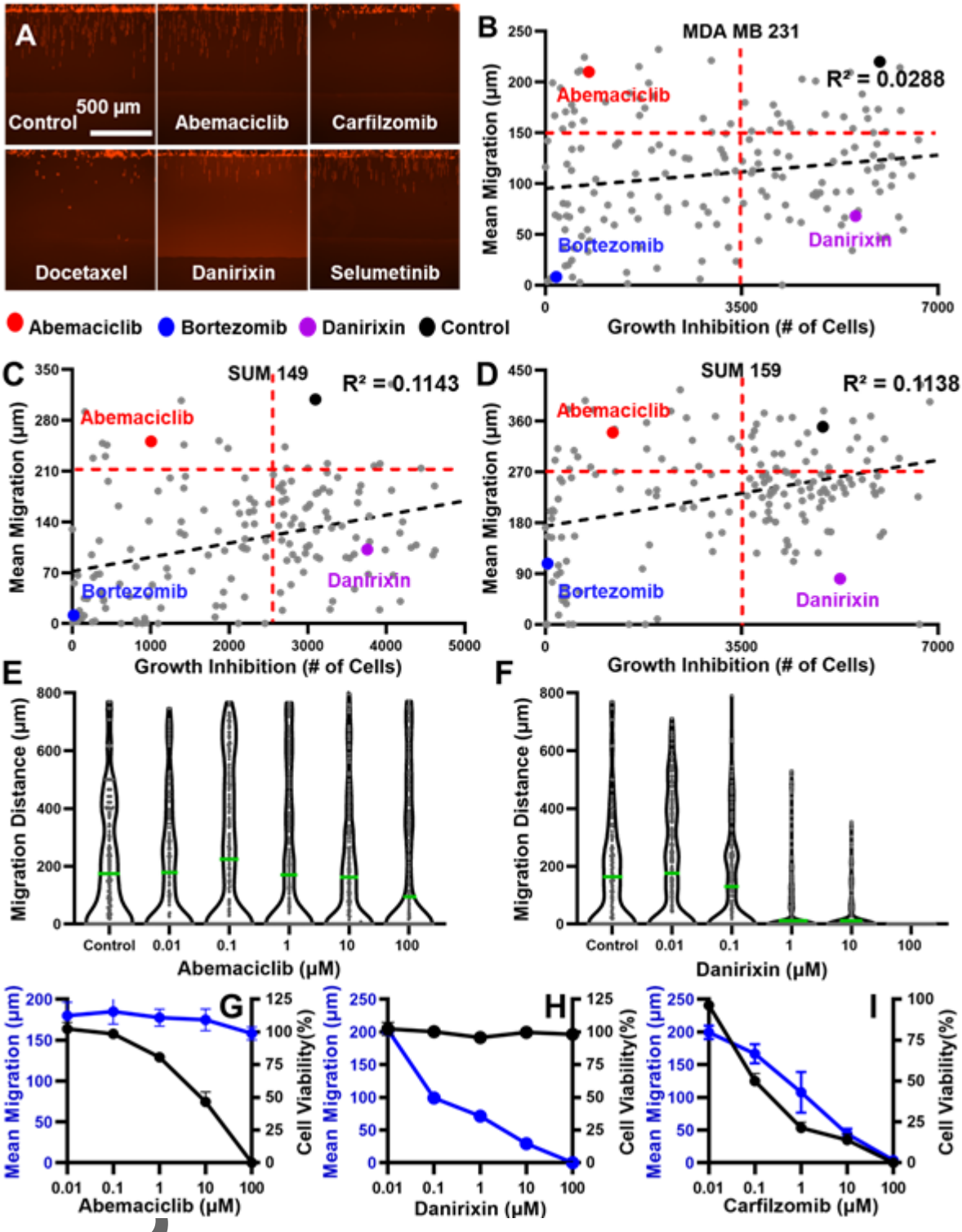

Figure 2. Correlation between the inhibition of cell growth and migration. (A) Representative images of MDA-MB-231 cells treated with DMSO control, Abemaciclib, Carfilzomib, Docetaxel, Danirixin, and Selumetinib (10 µM for all compounds). Scale bar: 500 µm. (B, C, D). Correlation between the inhibition of cell growth and migration for (B) MDA-MB-231, (C) SUM149, and (D) SUM159 cell lines with Pearson's correlation coefficients: MDA-MB-231 (R^2 = 0.0288), SUM149 (R^2 = 0.1143), SUM159 (R^2 = 0.1138).

The X-axis represents the number of cells after treatment, and the Y-axis represents the mean cell migration distance (μm)**.** Each dot represents one compound. The red dot represents Abemaciclib treatment, the blue dot represents Bortezomib treatment, and the purple dot represents Danirixin treatment. Statistical analysis is provided in Table S4, S5. (E, F). Treatments of selected compounds (Abemaciclib and Danirixin) at 6 concentrations (100 μM, 10 μM, 1 μM, 0.1 μM, 0,01 μM, and DMSO control) on MDA-MB-231 cells. The X-axis represents the concentration of the compound, and the Y-axis represents cell migration distance. The green bars represent the mean cell motility. N = 200 channels. (G, H, I). Treatments of selected compounds (Abemaciclib, Danirixin, and Carfilzomib) at 5 concentrations (100 μM, 10 μM, 1 μM, 0.1 μM, and 0,01 μM) on MDA-MB-231 cells. The Left Y-axis (blue) represents the migration distance, and the right Y-axis (black) represents the cell viability. The blue curve indicates the mean migration distance, and the black curve indicates the cell viability. Error bars indicate the standard error of the mean (SEM), n = 3.

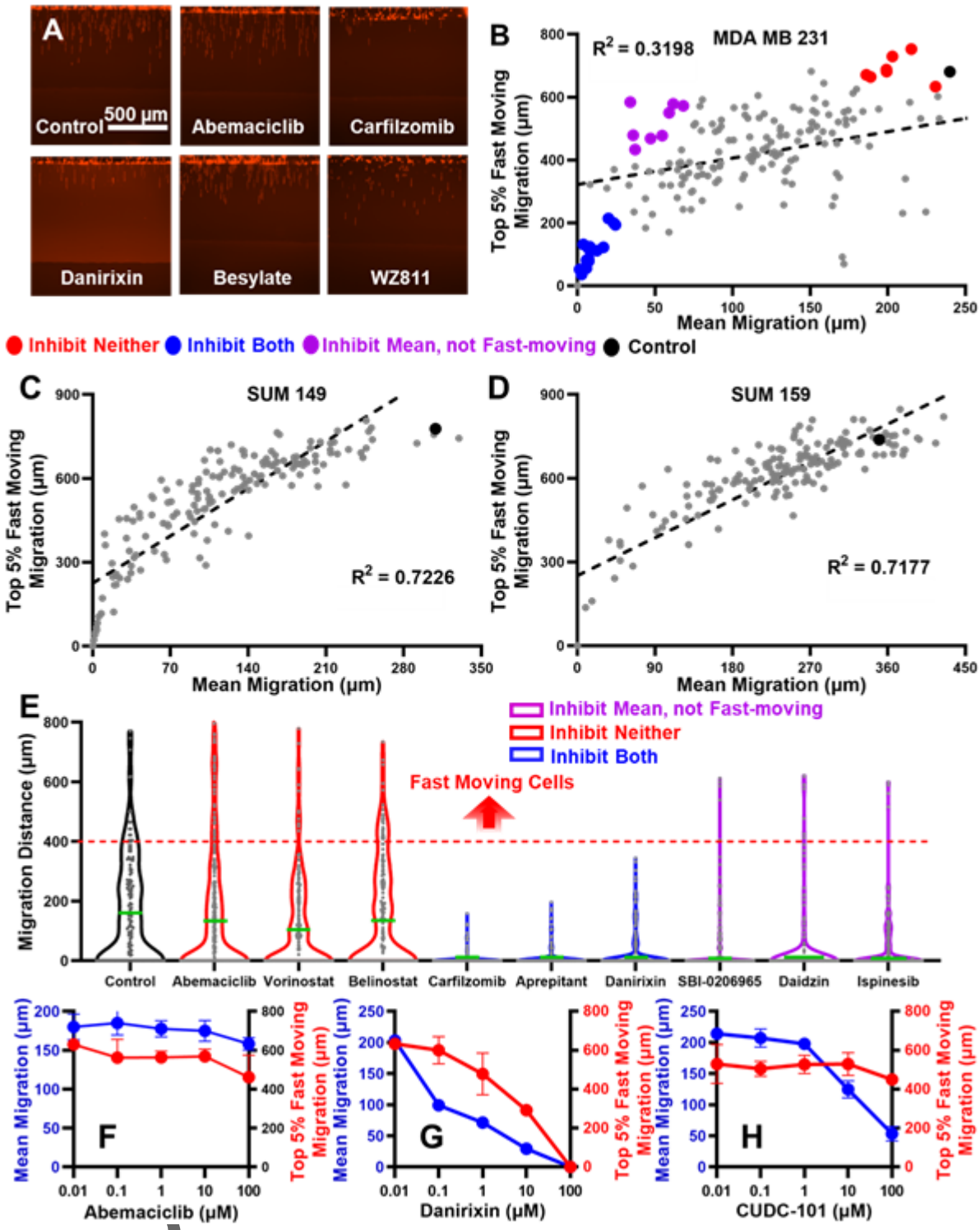

Figure 3. Correlation between the motility of mean and top-ranked fast-moving cells. (A) Representative images of MDA-MB-231 treated with DMSO control, Abemaciclib, Carfilzomib, Danirixin, Besylate, and WZ811 (10 µM for all compounds). Scale bar: 500 µm. (B, C, D). Correlation between the motility of mean and top-ranked fast-moving cells of (B) MDA-MB-231, (C) SUM149, and (D) SUM159 cell lines with Pearson's correlation coefficients: MDA-MB-231 (R^2 = 0.3198), SUM149 (R^2 = 0.7226), SUM159 (R^2 = 0.7177).

The X-axis represents the mean migration (μm) after treatment, and the Y-axis represents the top-ranked fast-moving migration distance (μm). Each dot represents one compound treatment. Different colors indicate different groups of compounds. The blue dots represent compounds that inhibited the migration of mean and top-ranked fast-moving cells, the red dots represent compounds that inhibited neither, the purple dots inhibited the migration of most cells but not the fast-moving ones, and the black dot represents DMSO control. Statistical analysis is provided in Table S7. (E) The distribution of migration distance for individual MDA-MB-231 cells treated with selected compounds (10 μM). The Y-axis represents cell migration distance. (μm). The green bars represent the mean cell motility. N = 200 channels. (F, G, H). Treatments of selected compounds (Abemaciclib, Danirixin, and CUDC-101) at 5 concentrations (100 μM, 10 μM, 1 μM, 0.1 μM, and 0,01 μM) on MDA-MB-231 cells. The Left Y-axis (blue) represents the mean migration distance, and the right Y-axis (red) represents the top 5% fast-moving cell migration distance. (μm). Error bars indicate the standard error of the mean (SEM), n = 3.

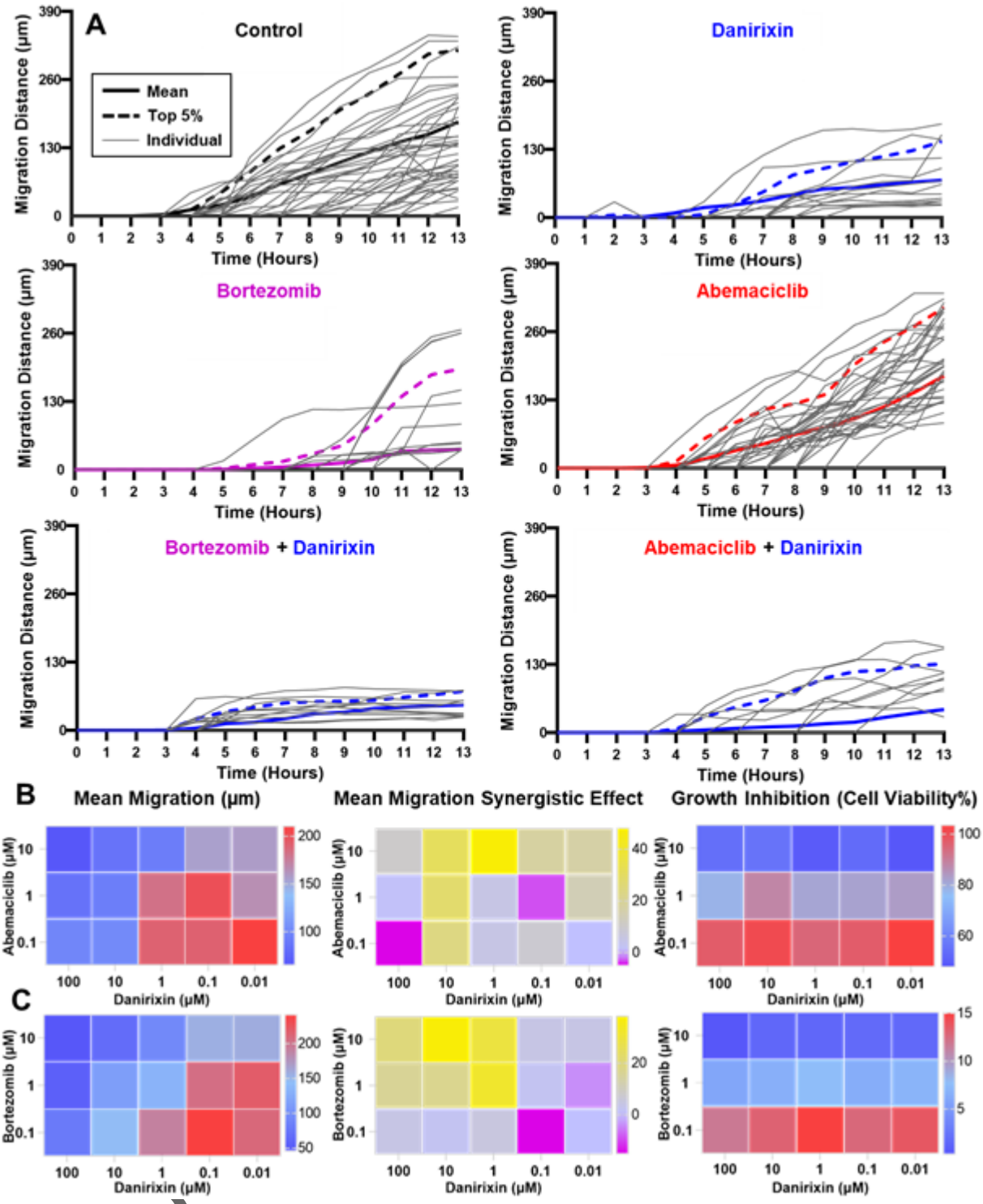

Figure 4. Dynamics of cell movement and the combination treatments of compounds

(A). Dynamics of cell migration. MDA-MB 231 cells with selected compound treatments were imaged every hour for 13 hours. The X-axis represents time (hours), and the Y-axis represents the migration distances (μm). The solid curve represents the mean migration distance, the dashed curve represents the top 5% fast-moving migration distance, and the gray thin solid curve represents the movement of individual cells. N = 300 channels. Six

conditions of DMSO control, Danirixin, Bortezomib, Abemaciclib, Bortezomib+Danirixin, and Abemaciclib+Danirixin (10 μM for all compounds) were tested. (B, C). The combinatory effects on migration and cell viability. (B) Abemaciclib (C) Bortezomib at three concentrations (10 μM, 1 μM, 0.1 μM) combined with Danirixin at 5 concentrations (100 μM, 10 μM, 1 μM, 0.1 μM, and 0,01 μM).

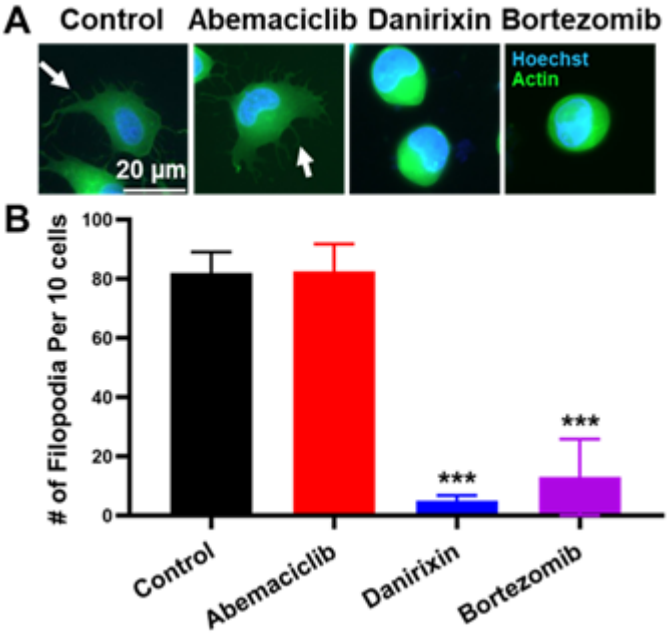

Figure 5. Cellular Filopodia are correlated with cell motility. (A) Representative images of MDA-MB-231 cells treated with DMSO control, Abemaciclib, Danirixin, and Bortezomib (10 μM for all compounds). Blue fluorescence represents Hoechst staining, and green fluorescence represents GFP-Actin. Scale bar: 20 μm. (B). The number of MDA-MB-231 cellular filopodia. The X-axis indicates the treatments. The Y-axis indicates the number of filopodia in every 10 cells. Statistical analysis is provided in Table S9. *** refers to $P < 0.001$ Error bars indicate the standard error of the mean (SEM), n = 4.

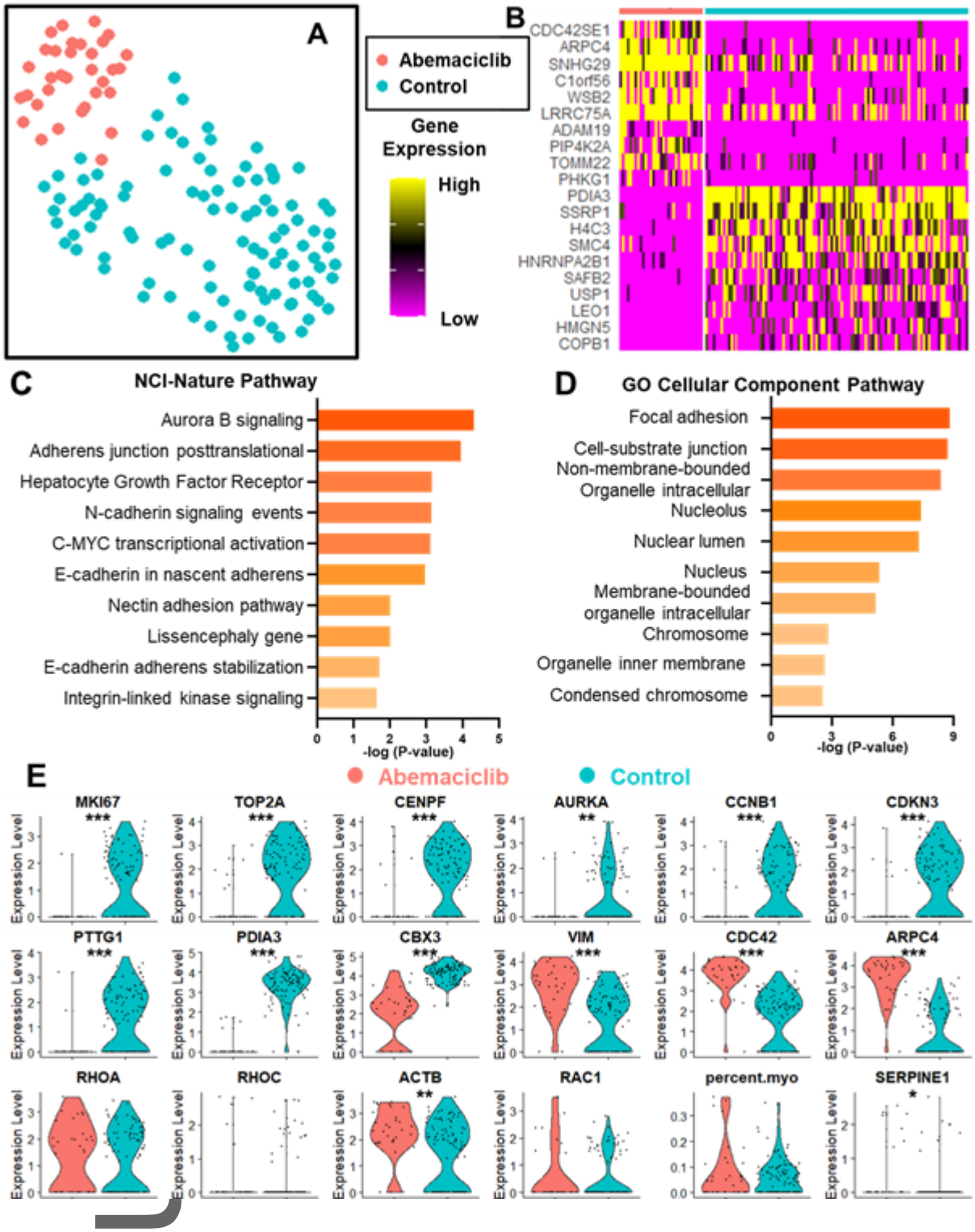

Figure 6. Single-cell transcriptome analysis of MDA-MB-231 with or without Abemaciclib treatment (A) UMAP plot of single-cell transcriptome analysis, MDA-MB-231 cells with and without Abemaciclib treatment. The X-axis represents UMAP1, the Y-axis represents UMAP2, and each dot represents one cell. Blue dots represent 105 control untreated cells, and red dots represent 33 Abemaciclib treated cells. (B) Heatmap demonstrates the significant gene expression differences between treated and untreated

MDA-MB-231 cells. (C, D). Top-ranked pathways determined by the altered genes of MDA-MB-231 cells treated with Abemaciclib versus control. The X-axis and color represent the p-values, and the Y-axis indicates the names of pathways. (C) the NCI-Nature pathway database and (D) the GO Cellular Component pathway database. (E) Violin plots of Abemaciclib treated and control MDA-MB-231 cells with statistical tests. The Y-axis represents gene expression with a logarithmic scale. Each dot represents one cell. * Refers to $P < 0.05$. ** refers to $P < 0.01$, and *** refers to $P < 0.001$.

Methods

Cell culture

We cultured MDA-MB-231 cells in Dulbecco's modified eagle medium (DMEM, Gibco 11995) supplemented with 10% fetal bovine serum (FBS, Gibco 16000), 1% GlutaMax (Gibco 35050), 1% penicillin/streptomycin (pen/strep, Gibco 15070), and 0.1% of plasmocin (InvivoGen ant-mpp). We cultured SUM149 and SUM159 cells in F-12 (Gibco 11765) media supplemented with 5% FBS (Gibco 16000), 1% pen/strep (Gibco 15070), 1% GlutaMax (Gibco 35050), 1 μg mL^{-1} hydrocortisone (Sigma H4001), and 5 μg mL^{-1} insulin (Sigma I6634), and 0.1% of plasmocin (InvivoGen, ant-mpp). MDA-MB-231, SUM149, and SUM159 cells were obtained from Dr. Gary Luker's lab at the University of Michigan. We maintained all cells at 37 °C in a humidified incubator with 5% CO2. All the cells were cultured and passaged when the cells reached over 80% confluency in the dish.

Cell transfection

We stably transfected TNBC cells using Xfect™ Transfection Reagent (Takara 631317) with 5 μg of pEF1alpha-tdTomato Vector plasmid (Takara 631975). The cells labeled with red fluorescent proteins can be tracked for migration. The transfected cells were selected using G418 (Takara 631307) treatment and sorted by flow cytometry for red fluorescence. We previously described cells stably transduced with LifeAct-GFP to visualize actin.[75,87]

Microfluidic chip design and fabrication

The migration devices were fabricated from a single layer of PDMS (Polydimethylsiloxane, Sylgard 184, Dow Corning), which was fabricated on a silicon wafer by standard soft lithography. One mask was used to fabricate the migration channel (5 μm height). One device contains 3,200 migration channels (100 channels per pair of wells), and the migration channel is 10 μm in width, 5 μm in height, and 1 mm in length. The size of a device is 75.8 mm by 25 mm, and the pitch between wells is 4.5 mm (following the 384-well plate format). The microfabrication was performed by MuWells Inc. The patterned PDMS layer was

bonded to the ProPlate® 64-Well Chambers (246855, Grace Bio-Labs) after being activated by oxygen plasma treatment (Plasma Oven, PDC-001, Harrick Plasma) for 5 mins to form a complete fluidic channel. After bonding, the devices were heated at 80ºC for 15 minutes to ensure bonding quality. The microfluidic chips were sanitized by UV radiation prior to use to ensure sterile conditions. Before cell loading, Collagen (1.45mL Collagen (Collagen Type 1, 354236, BD Biosciences), 0.1mL acetic acid in 50mL DI Water) was coated overnight on the device to enhance cell adhesion. Devices were then rinsed with cell culture media before usage to remove the residual collagen solution.

Cell migration assay

A library of 172 compounds was selected for the screening experiments based on their functions in literature as listed in **Table S3**. The compounds were dissolved to 10 mM in either DMSO or PBS according to the instructions from the vendors. Compound solutions were prepared by serial dilution, and the final concentration of 10 μM was used in the screening experiments. DMSO (0.01%) treatment was used as the control. Cells were harvested from culture plates with 0.05% Trypsin/EDTA (Gibco, 25200) and centrifuged at 1000 rpm for 4 mins. Then, the cells were re-suspended in culture media to a concentration of 4.17 x 10^5 cells/mL (2.5 x 10^4 cells per well). 60 μL of this cell suspension was pipetted into the upper wells and 20 μL of culture media was pipetted into the lower wells. Trypsinized rounded cells (diameter: 10–15 μm) were larger than the migration channel height (5 μm), so they were initially trapped at the entrance of migration channels. The device maintained a static flow condition and stayed in an incubator for 30 minutes to enhance cell adhesion on the substrate, and we visually confirmed cell adhesion morphology before doing the next step. After visual inspection, cell suspension in the upper wells was aspirated and replaced with 60 μL serum-free culture media with treatment compounds (10 μM). The lower wells will be added to 60 μL serum culture media with treatment compounds (10 μM) to induce chemotactic migration toward serum. Due to the nature of diffusion, the concentration of the chemoattractant in the migration channel increases linearly along the channel from the cell loading side. The detailed simulation and measurement were discussed in our previous works.[14,15] Then, the device was put into a cell culture incubator. Migration distance was measured based on the final cell frontier (the cell migrating the farthest) of each migration channel after 24 hours of incubation without media replenishment.

Growth inhibition assay

Cells were harvested from cell culture dishes with 0.05% Trypsin/EDTA (Gibco 25200) and centrifuged at 1,000 rpm for 4 minutes. Then, the cells were re-suspended in the cell culture

media for seeding into 96-well plates. For SUM149 cells, 2,000 cells in 100 µL media were seeded per well. For SUM159 and MDA-MB-231 cells, 1,000 cells in 100 µL media were seeded per well. Loaded cells were cultured for 24 hours and then treated with compounds for 48 hours. Cells were then stained by 0.8 µM Calcein AM, 1.6 µM Ethidium homodimer-1 (Invitrogen™ L3224 Live/Dead Viability/Cytotoxicity Kit), and 5 µM Hoechst 33342 (Thermo Scientific 62249) for 30 minutes in the incubator and imaged. The Hoechst staining image was first filtered by top-hat and bottom-hat filters to reduce the background, enhanced by contract adjustment, and binarized to quantify the size of nuclei. Cell debris were excluded by their smaller sizes. Live/Dead staining was used to exclude dead cells with dim live signals and bright dead signals. The custom MATLAB program for cell counting was developed based on our previous works.[88,89]

Transwell assay

Nunc Polycarbonate Cell Culture Inserts, 8 µm pore size (Thermo Scientific™ 140644) were used for Transwell migration assays. Cell culture media (2 mL per well) with serum was added to 6-well plates, and 7.5 x 10^4 cells in 1 mL of serum-free media were added to Transwell inserts. After 30 minutes, compound treatments of 10 µM were applied. Then, the Transwell plate was put into a cell culture incubator. After 24 hours, cells on the lower surface of the inserts were stained with 5 µM Hoechst 33342 (Thermo Scientific 62249), 0.8 µM Calcein AM (Invitrogen™ L3224) for 30 minutes. After washing 3 times with PBS (Gibco 10010) to eliminate cells on the top surface and the residual dye, the inserts were observed and photographed under a microscope.

Image acquisition

The microfluidic chips were imaged using an inverted microscope (Nikon Ti2-E). The brightfield and fluorescence images were taken with a 40x, 10x, or 4x objective lens and a monochrome CMOS camera (Hamamatsu ORCA-Fusion Gen-III SCMOS Camera). The field of view is around 14 mm^2, which can cover 100 cell migration channels in an image. The outline of the device was fluorescently imaged by a DAPI filter set, transfected RFP cells were fluorescently imaged by a mCherry filter set, and Actin-GFP cells were imaged by a FITC filter set. Auto focusing was performed to ensure the image remained in focus throughout the imaging experiments. It takes less than 10 minutes to image a migration device that tests 32 conditions. The time-lapse experiments to monitor cell population dynamics were performed using a Tokai Hit stage top environment control on the Nikon Ti2-E microscope.

Autonomous image analysis for monitoring cellular migration

To process thousands of images in this study, we established an autonomous image processing toolkit (MATLAB 2021b) with fully automatic image registration and quality control functions. The image registration was performed using two features on the images. (1) The blue auto-fluorescence of Silicone on the ProPlate® 64-Well device was used to identify the region of cell migration channel. (2) The brightfield image of migration channels was used to calculate the rotation angles and separate individual channels. (**Fig. 1**) As the patterns of migration channels extend beyond the core cell migration area, the patterns are recognizable by brightfield imaging. Based on those two features, the images can be automatically cropped and rotated for registration. In addition, we implemented quality control functions to exclude images from defective microfluidic devices and poor imaging conditions. The migration devices with leakage, trapped bubbles were excluded. The over-exposed and out-of-focus images were also eliminated automatically. On average, around 20% of images were excluded. After quality control, the migration channels were identified, and the location of cells was calculated based on cellular fluorescence. Point noise, debris, and dead cells were excluded by their small area and dim fluorescence. In each migration channel, the program marked the live cells that move farthest as the migration frontier in that channel. We have validated the software by comparing manual and computer-aided cell identification. The autonomous image analysis successfully excluded all defective images, and the location of recognized cells was consistent with the manual identification.

Single-cell RNA-Seq

We performed high-throughput single-cell barcoding transcriptome sequencing for MDA-MB-231 cells with and without Abemaciclib treatment.[90-92] Cells were cultured in a 6-well plate Corning™ 3516, treated with Abemaciclib for 24 hours (the same as the migration experiment), and harvested with 0.05% Trypsin/EDTA (Gibco 25200) for scRNA-Seq. We are aware that the microenvironment in the microfluidic channels is not the same as that in a 6-well plate. However, as it is difficult to retrieve cells directly from the enclosed migration channels, we cultured treated and untreated cells in a 6-well plate for side-by-side comparison. Cells and beads were paired in microwells, so the mRNA from lysed cells can hybridize onto the barcoded beads. After barcoded beads captured cellular mRNA, we performed RT (Thermofisher Maxima RT kit), PCR (Kapa HiFi Hotstart PCR Readymix), and library preparation (Illumina Nextera XT Library Prep Kit). The cDNA samples were then quantified and pooled by the UPMC Cancer Genome Core for sequencing using the Illumina NextSeq. We obtained approximately 10 million paired-end reads (Read 1: 30 base pairs for the barcode and Read 2: 250 base pairs for mRNA read alignment) for each population. Reads were aligned using STAR with GRCh38.p13 Human reference genome and

processed by the standard Dropseq 2.5.1 pipeline. Then, we used the open-source SEURAT 4.0 (http://satijalab.org/seurat/) to analyze single-cell sequencing data.[93] Cells with more than 500 genes detected were considered successfully sequenced, and the cells having more than 5% mitochondrial gene expression were discarded for their poor viability.

Statistical analysis

We performed statistical analysis using R (version 4.1), GraphPad Prism 9, Combenefit (version 2.021), and MATLAB. Half-maximal inhibitory concentrations (IC50s) were determined using GraphPad Prism 9 software. Comparisons of two different groups were performed by the two-tailed Student's t-test. Multiple groups were compared using 2-way ANOVA (cell line and treatment condition are two variables) Fisher's Least Significant Difference (LSD) test. Synergistic effects were calculated using the Combenefit software.[94] The exact statistical setups were determined depending on the variable types and nature of analysis. We used $p<0.05$ to define statistically significant differences for all analyses. * Refers to $P < 0.05$, ** refers to $P < 0.01$, and *** refers to $P < 0.001$. Standard error of the mean (SEM) was used for designating error bars. The number of samples or groups used was provided in the Figure Captions. The correlation coefficients were calculated based on the Pearson correlation using GraphPad Prism. For measurements with high variability (such as gene expression levels), we compared these data on a log scale. For single-cell transcriptome sequencing data, we used the R package SEURAT for data analysis, such as outlier detection, hierarchical clustering, principal component analysis (PCA), and Uniform Manifold Approximation and Projection (UMAP).[93] To compare cell populations, we identified altered genes defined by logarithmic fold change of 0.25 and the minimal portion of expressing cells of 10% for pathway analysis. Pathway analysis was performed using Enrichr (http://amp.pharm.mssm.edu/Enrichr/) tool with the GO Cellular Component and NCI-Nature databases.[95] The p-values in pathway analysis were generated using Fisher exact tests by Enrichr.

Data Availability

The authors declare that all relevant data are included in the main text and/or its supplementary information files. Source data will be available in the Source Data file. The single-cell RNA-Seq data will be deposited and available in the Sequence Read Archive (SRA) once the manuscript is published.

Acknowledgments

This study was generously supported by start-up funding from the UPMC Hillman Cancer Center, the Women's Cancer Research Center (WCRC) at Magee Women's Research Institute, and the Pitt CTSI Pilot project (This project was supported by the National Institutes of Health through Grant Number UL1TR001857.) to Y.-C.C. M.Z. was partially supported by the Xiangya visiting scholar program. G.D.L. acknowledges funding from US NIH grants R01 CA238023, U24 CA237683, R01 CA238042, U01 CA210152, R33 CA225549, and R37 CA222563. K.E.L. acknowledges funding from R50 CA221807. G.D.L. and K.E.L. also acknowledge funding from the W.M. Keck Foundation. We thank the Nanoscale Fabrication Characterization Facility of the University of Pittsburgh (Pittsburgh, PA) for device fabrication and Drs. Adrian Lee and Steffi Oesterreich (University of Pittsburgh) for insightful discussion.

Author Contributions

M.Z. and Y.-C.C. performed the fabrication of microfluidic devices. M.Z. and Y.-C.C. performed the cell migration experiments. Y.M. developed the software for image processing. C.-C.C. and Y.-C.C. performed the single-cell RNA-Seq experiments. E.C.R. and Y.-C.C. performed the sequencing read alignment and data analysis. K.E.L., G.D.L., and Y.-C.C. performed cell transfection and transduction. Y.-C.C. supervised the study. M.Z., and Y.-C.C. wrote the manuscript. All authors discussed the results and commented on the manuscript.

Competing Interests

The authors declare no competing interests.

References

1. Hanahan, D. & Weinberg, A., Robert. Hallmarks of Cancer: The Next Generation. *Cell* **144**, 646-674 (2011).
2. Steeg, P.S. Tumor metastasis: mechanistic insights and clinical challenges. *Nat Med* **12**, 895-904 (2006).
3. Bravo-Cordero, J.J., Hodgson, L. & Condeelis, J. Directed cell invasion and migration during metastasis. *Curr Opin Cell Biol* **24**, 277-283 (2012).
4. Frank, N.Y., Schatton, T. & Frank, M.H. The therapeutic promise of the cancer stem cell concept. *J Clin Invest* **120**, 41-50 (2010).
5. Kreso, A. & Dick, J.E. Evolution of the cancer stem cell model. *Cell Stem Cell* **14**, 275-291 (2014).
6. Brooks, M.D., Burness, M.L. & Wicha, M.S. Therapeutic Implications of Cellular Heterogeneity and Plasticity in Breast Cancer. *Cell Stem Cell* **17**, 260-271 (2015).

7. Mani, S.A., *et al.* The epithelial-mesenchymal transition generates cells with properties of stem cells. *Cell* **133**, 704-715 (2008).

8. Ye, X., *et al.* Distinct EMT programs control normal mammary stem cells and tumour-initiating cells. *Nature* **525**, 256-260 (2015).

9. Ye, X. & Weinberg, R.A. Epithelial-Mesenchymal Plasticity: A Central Regulator of Cancer Progression. *Trends Cell Biol* **25**, 675-686 (2015).

10. Lee, E., *et al.* DNMT1 Regulates Epithelial-Mesenchymal Transition and Cancer Stem Cells, Which Promotes Prostate Cancer Metastasis. *Neoplasia* **18**, 553-566 (2016).

11. Guo, W., *et al.* Slug and Sox9 cooperatively determine the mammary stem cell state. *Cell* **148**, 1015-1028 (2012).

12. Roy, S.S., *et al.* Significance of PELP1/HDAC2/miR-200 regulatory network in EMT and metastasis of breast cancer. *Oncogene* **33**, 3707-3716 (2014).

13. Tran, H.D., *et al.* Transient SNAIL1 expression is necessary for metastatic competence in breast cancer. *Cancer Res* **74**, 6330-6340 (2014).

14. Chen, Y.C., *et al.* Single-cell Migration Chip for Chemotaxis-based Microfluidic Selection of Heterogeneous Cell Populations. *Sci Rep* **5**, 9980 (2015).

15. Chen, Y.C., *et al.* Functional Isolation of Tumor-Initiating Cells using Microfluidic-Based Migration Identifies Phosphatidylserine Decarboxylase as a Key Regulator. *Sci Rep* **8**, 244 (2018).

16. Chen, Y.C., *et al.* Single-cell RNA-sequencing of migratory breast cancer cells: discovering genes associated with cancer metastasis. *Analyst* **144**, 7296-7309 (2019).

17. Yankaskas, C.L., *et al.* A microfluidic assay for the quantification of the metastatic propensity of breast cancer specimens. *Nat Biomed Eng* **3**, 452-465 (2019).

18. Wong, B.S., *et al.* A microfluidic cell-migration assay for the prediction of progression-free survival and recurrence time of patients with glioblastoma. *Nat Biomed Eng* **5**, 26-40 (2021).

19. Shoemaker, R.H. The NCI60 human tumour cell line anticancer drug screen. *Nat Rev Cancer* **6**, 813-823 (2006).

20. Alday-Parejo, B., Stupp, R. & Ruegg, C. Are Integrins Still Practicable Targets for Anti-Cancer Therapy? *Cancers (Basel)* **11**(2019).

21. Bergonzini, C., Kroese, K., Zweemer, A.J.M. & Danen, E.H.J. Targeting Integrins for Cancer Therapy - Disappointments and Opportunities. *Front Cell Dev Biol* **10**, 863850 (2022).

22. Koltai, T. Nelfinavir and other protease inhibitors in cancer: mechanisms involved in anticancer activity. *F1000Res* **4**, 9 (2015).

23. Rudzinska, M.*, et al.* Current Status and Perspectives of Protease Inhibitors and Their Combination with Nanosized Drug Delivery Systems for Targeted Cancer Therapy. *Drug Des Devel Ther* **15**, 9-20 (2021).

24. Huang, J.*, et al.* Extracellular matrix and its therapeutic potential for cancer treatment. *Signal Transduct Target Ther* **6**, 153 (2021).

25. Henke, E., Nandigama, R. & Ergun, S. Extracellular Matrix in the Tumor Microenvironment and Its Impact on Cancer Therapy. *Front Mol Biosci* **6**, 160 (2019).

26. Altschuler, S.J. & Wu, L.F. Cellular heterogeneity: do differences make a difference? *Cell* **141**, 559-563 (2010).

27. Carter, B. & Zhao, K. The epigenetic basis of cellular heterogeneity. *Nat Rev Genet* **22**, 235-250 (2021).

28. Meacham, C.E. & Morrison, S.J. Tumour heterogeneity and cancer cell plasticity. *Nature* **501**, 328-337 (2013).

29. McGranahan, N. & Swanton, C. Clonal Heterogeneity and Tumor Evolution: Past, Present, and the Future. *Cell* **168**, 613-628 (2017).

30. You, J.S. & Jones, P.A. Cancer genetics and epigenetics: two sides of the same coin? *Cancer Cell* **22**, 9-20 (2012).

31. Torgovnick, A. & Schumacher, B. DNA repair mechanisms in cancer development and therapy. *Front Genet* **6**, 157 (2015).

32. Whiteside, T.L. The tumor microenvironment and its role in promoting tumor growth. *Oncogene* **27**, 5904-5912 (2008).

33. Dagogo-Jack, I. & Shaw, A.T. Tumour heterogeneity and resistance to cancer therapies. *Nat Rev Clin Oncol* **15**, 81-94 (2018).

34. Prasetyanti, P.R. & Medema, J.P. Intra-tumor heterogeneity from a cancer stem cell perspective. *Mol Cancer* **16**, 41 (2017).

35. Rodriguez, L.G., Wu, X. & Guan, J.L. Wound-healing assay. *Methods Mol Biol* **294**, 23-29 (2005).

36. Chen, H.C. Boyden chamber assay. *Methods Mol Biol* **294**, 15-22 (2005).

37. Xie, Y.*, et al.* A microchip-based model wound with multiple types of cells. *Lab Chip* **11**, 2819-2822 (2011).

38. Irimia, D., Charras, G., Agrawal, N., Mitchison, T. & Toner, M. Polar stimulation and constrained cell migration in microfluidic channels. *Lab Chip* **7**, 1783-1790 (2007).

39. Shin, M.K., Kim, S.K. & Jung, H. Integration of intra- and extravasation in one cell-based microfluidic chip for the study of cancer metastasis. *Lab Chip* **11**, 3880-3887 (2011).

40. Yan, J. & Irimia, D. Stochastic variations of migration speed between cells in clonal populations. *Technology (Singap World Sci)* **2**, 185-188 (2014).

41. Bajpai, S., Mitchell, M.J., King, M.R. & Reinhart-King, C.A. A microfluidic device to select for cells based on chemotactic phenotype. *Technology (Singap World Sci)* **2**, 101-105 (2014).

42. Irimia, D. & Toner, M. Spontaneous migration of cancer cells under conditions of mechanical confinement. *Integr Biol (Camb)* **1**, 506-512 (2009).

43. Mak, M., Reinhart-King, C.A. & Erickson, D. Microfabricated physical spatial gradients for investigating cell migration and invasion dynamics. *PLoS One* **6**, e20825 (2011).

44. Gallego-Perez, D.*, et al.* Microfabricated mimics of in vivo structural cues for the study of guided tumor cell migration. *Lab Chip* **12**, 4424-4432 (2012).

45. Ko, Y.G., Co, C.C. & Ho, C.C. Gradient-free directional cell migration in continuous microchannels. *Soft Matter* **9**, 2467-2474 (2013).

46. Dent, R.*, et al.* Triple-negative breast cancer: clinical features and patterns of recurrence. *Clin Cancer Res* **13**, 4429-4434 (2007).

47. Al-Mahmood, S., Sapiezynski, J., Garbuzenko, O.B. & Minko, T. Metastatic and triple-negative breast cancer: challenges and treatment options. *Drug Deliv Transl Res* **8**, 1483-1507 (2018).

48. Venere, M.*, et al.* The mitotic kinesin KIF11 is a driver of invasion, proliferation, and self-renewal in glioblastoma. *Sci Transl Med* **7**, 304ra143 (2015).

49. Cayetano-Salazar, L.*, et al.* Natural isoflavonoids in invasive cancer therapy: From bench to bedside. *Phytother Res* **35**, 4092-4110 (2021).

50. Chan, K.K.L.*, et al.* Estrogen receptor modulators genistein, daidzein and ERB-041 inhibit cell migration, invasion, proliferation and sphere formation via modulation of FAK and PI3K/AKT signaling in ovarian cancer. *Cancer Cell Int* **18**, 65 (2018).

51. Tang, F.*, et al.* SBI0206965, a novel inhibitor of Ulk1, suppresses non-small cell lung cancer cell growth by modulating both autophagy and apoptosis pathways. *Oncol Rep* **37**, 3449-3458 (2017).

52. Ha, H., Debnath, B. & Neamati, N. Role of the CXCL8-CXCR1/2 Axis in Cancer and Inflammatory Diseases. *Theranostics* **7**, 1543-1588 (2017).

53. Munoz, M.*, et al.* The neurokinin-1 receptor antagonist aprepitant is a promising candidate for the treatment of breast cancer. *Int J Oncol* **45**, 1658-1672 (2014).

54. Kubiczkova, L., Pour, L., Sedlarikova, L., Hajek, R. & Sevcikova, S. Proteasome inhibitors - molecular basis and current perspectives in multiple myeloma. *J Cell Mol Med* **18**, 947-961 (2014).

55. Lai, C.J., *et al.* CUDC-101, a multitargeted inhibitor of histone deacetylase, epidermal growth factor receptor, and human epidermal growth factor receptor 2, exerts potent anticancer activity. *Cancer Res* **70**, 3647-3656 (2010).

56. Al-Lazikani, B., Banerji, U. & Workman, P. Combinatorial drug therapy for cancer in the post-genomic era. *Nat Biotechnol* **30**, 679-692 (2012).

57. Vasioukhin, V., Bauer, C., Yin, M. & Fuchs, E. Directed actin polymerization is the driving force for epithelial cell-cell adhesion. *Cell* **100**, 209-219 (2000).

58. Davis, J.R., *et al.* Inter-cellular forces orchestrate contact inhibition of locomotion. *Cell* **161**, 361-373 (2015).

59. Zhang, H., *et al.* Myosin-X provides a motor-based link between integrins and the cytoskeleton. *Nat Cell Biol* **6**, 523-531 (2004).

60. Miller, I., *et al.* Ki67 is a Graded Rather than a Binary Marker of Proliferation versus Quiescence. *Cell Rep* **24**, 1105-1112 e1105 (2018).

61. Neubauer, E., *et al.* Comparative evaluation of three proliferation markers, Ki-67, TOP2A, and RacGAP1, in bronchopulmonary neuroendocrine neoplasms: Issues and prospects. *Oncotarget* **7**, 41959-41973 (2016).

62. Nikonova, A.S., Astsaturov, I., Serebriiskii, I.G., Dunbrack, R.L., Jr. & Golemis, E.A. Aurora A kinase (AURKA) in normal and pathological cell division. *Cell Mol Life Sci* **70**, 661-687 (2013).

63. Fang, Y., Yu, H., Liang, X., Xu, J. & Cai, X. Chk1-induced CCNB1 overexpression promotes cell proliferation and tumor growth in human colorectal cancer. *Cancer Biol Ther* **15**, 1268-1279 (2014).

64. Liu, J., *et al.* Cyclin-Dependent Kinase Inhibitor 3 Promoted Cell Proliferation by Driving Cell Cycle from G1 to S Phase in Esophageal Squamous Cell Carcinoma. *J Cancer* **10**, 1915-1922 (2019).

65. Noll, J.E., *et al.* PTTG1 expression is associated with hyperproliferative disease and poor prognosis in multiple myeloma. *J Hematol Oncol* **8**, 106 (2015).

66. Battaglia, R.A., Delic, S., Herrmann, H. & Snider, N.T. Vimentin on the move: new developments in cell migration. *F1000Res* **7**(2018).

67. Raftopoulou, M. & Hall, A. Cell migration: Rho GTPases lead the way. *Dev Biol* **265**, 23-32 (2004).

68. Ridley, A.J. Rho GTPase signalling in cell migration. *Curr Opin Cell Biol* **36**, 103-112 (2015).

69. Xu, N., *et al.* ARPC4 promotes bladder cancer cell invasion and is associated with lymph node metastasis. *J Cell Biochem* **121**, 231-243 (2020).

70. O'Connor, K. & Chen, M. Dynamic functions of RhoA in tumor cell migration and invasion. *Small GTPases* **4**, 141-147 (2013).

71. Vega, F.M., Fruhwirth, G., Ng, T. & Ridley, A.J. RhoA and RhoC have distinct roles in migration and invasion by acting through different targets. *J Cell Biol* **193**, 655-665 (2011).

72. Allen, S.G.*, et al.* Macrophages Enhance Migration in Inflammatory Breast Cancer Cells via RhoC GTPase Signaling. *Sci Rep* **6**, 39190 (2016).

73. Katoh, H., Hiramoto, K. & Negishi, M. Activation of Rac1 by RhoG regulates cell migration. *J Cell Sci* **119**, 56-65 (2006).

74. Makowska, K.A., Hughes, R.E., White, K.J., Wells, C.M. & Peckham, M. Specific Myosins Control Actin Organization, Cell Morphology, and Migration in Prostate Cancer Cells. *Cell Rep* **13**, 2118-2125 (2015).

75. Humphries, B.A.*, et al.* Plasminogen Activator Inhibitor 1 (PAI1) Promotes Actin Cytoskeleton Reorganization and Glycolytic Metabolism in Triple-Negative Breast Cancer. *Mol Cancer Res* **17**, 1142-1154 (2019).

76. Ishizawa, K.*, et al.* Tumor-initiating cells are rare in many human tumors. *Cell Stem Cell* **7**, 279-282 (2010).

77. Yu, Z., Pestell, T.G., Lisanti, M.P. & Pestell, R.G. Cancer stem cells. *Int J Biochem Cell Biol* **44**, 2144-2151 (2012).

78. Vlashi, E. & Pajonk, F. Cancer stem cells, cancer cell plasticity and radiation therapy. *Semin Cancer Biol* **31**, 28-35 (2015).

79. Silva, I.A.*, et al.* Aldehyde dehydrogenase in combination with CD133 defines angiogenic ovarian cancer stem cells that portend poor patient survival. *Cancer Res* **71**, 3991-4001 (2011).

80. Campoy, E.M., Branham, M.T., Mayorga, L.S. & Roque, M. Intratumor heterogeneity index of breast carcinomas based on DNA methylation profiles. *BMC Cancer* **19**, 328 (2019).

81. Khan, G.N., Kim, E.J., Shin, T.S. & Lee, S.H. Heterogeneous Cell Types in Single-cell-derived Clones of MCF7 and MDA-MB-231 Cells. *Anticancer Res* **37**, 2343-2354 (2017).

82. Shen, Y.*, et al.* Detecting heterogeneity in and between breast cancer cell lines. *Cancer Converg* **4**, 1 (2020).

83. DeVita, V.T., Jr., Young, R.C. & Canellos, G.P. Combination versus single agent chemotherapy: a review of the basis for selection of drug treatment of cancer. *Cancer* **35**, 98-110 (1975).

84. Yardley, D.A. Drug resistance and the role of combination chemotherapy in improving patient outcomes. *Int J Breast Cancer* **2013**, 137414 (2013).

85. Macarron, R.*, et al.* Impact of high-throughput screening in biomedical research. *Nat Rev Drug Discov* **10**, 188-195 (2011).

86. Tang, J., *et al.* Target inhibition networks: predicting selective combinations of druggable targets to block cancer survival pathways. *PLoS Comput Biol* **9**, e1003226 (2013).

87. Zhang, Z., *et al.* Morphology-based prediction of cancer cell migration using an artificial neural network and a random decision forest. *Integr Biol (Camb)* **10**, 758-767 (2018).

88. Cheng, Y.H., Chen, Y.C., Brien, R. & Yoon, E. Scaling and automation of a high-throughput single-cell-derived tumor sphere assay chip. *Lab Chip* **16**, 3708-3717 (2016).

89. Chen, Y.C., Zhang, Z. & Yoon, E. Early Prediction of Single-Cell Derived Sphere Formation Rate Using Convolutional Neural Network Image Analysis. *Anal Chem* **92**, 7717-7724 (2020).

90. Macosko, E.Z., *et al.* Highly Parallel Genome-wide Expression Profiling of Individual Cells Using Nanoliter Droplets. *Cell* **161**, 1202-1214 (2015).

91. Gierahn, T.M., *et al.* Seq-Well: portable, low-cost RNA sequencing of single cells at high throughput. *Nat Methods* **14**, 395-398 (2017).

92. Cheng, Y.H., *et al.* Hydro-Seq enables contamination-free high-throughput single-cell RNA-sequencing for circulating tumor cells. *Nat Commun* **10**, 2163 (2019).

93. Hao, Y., *et al.* Integrated analysis of multimodal single-cell data. *Cell* **184**, 3573-3587 e3529 (2021).

94. Di Veroli, G.Y., *et al.* Combenefit: an interactive platform for the analysis and visualization of drug combinations. *Bioinformatics* **32**, 2866-2868 (2016).

95. Chen, E.Y., *et al.* Enrichr: interactive and collaborative HTML5 gene list enrichment analysis tool. *BMC Bioinformatics* **14**, 128 (2013).

Table of Contents

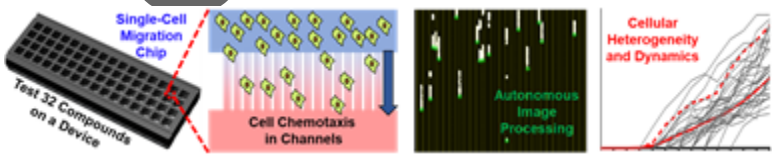

We established a high-throughput single-cell migration platform that coordinates robotic liquid handling and autonomous image processing for quantifying cellular heterogeneity and dynamics in migration. Using this innovative technology, we found a surprisingly low correlation between inhibition of cell migration and growth, and many compounds inhibited migration of most cells but not fast-moving subpopulations.